Cellulose (2023) 30:2037–2052
https://doi.org/10.1007/s10570-022-05026-2

ORIGINAL RESEARCH

Solution casting of cellulose acetate films: influence of surface substrate and humidity on wettability, morphology and optical properties

Ana Kramar · Irene Rodríguez Ortega · Gustavo González-Gaitano · Javier González-Benito

Received: 5 September 2022 / Accepted: 24 December 2022 / Published online: 9 January 2023

Abstract Variations on the processing conditions of conventional methods for polymeric film preparation may allow tuning certain properties. In this work, different casting surfaces and humidity are presented as variables to consider for cellulose acetate (CA) film preparation using conventional solution casting method. Specifically, borosilicate glass, soda-lime glass and Teflon (PTFE) dishes have been used for casting and their influence on various properties on CA films assessed. The surfaces of glass dishes are smooth, while PTFE surface has a pattern constituted by concentric channels of micro dimensions (as seen by optical microscope), which is adopted by cast films upon drying. The resulting patterned films are translucent while films produced using smooth surfaces are transparent. The effect of the environment humidity (35%, 55% and 75% RH) in the properties of the CA films during the evaporation of solvent from solution has been evaluated. Higher humidity produces smoother surfaces and increased crystallinity as shown by XRD and DSC; however, the wettability of the films does not seem to be influenced by this variable. Due to the specific morphology of the patterned films, changes in material opacity upon wetting are detected, from translucent to transparent, while the removal of water from the surface restores the translucency. This micropatterning effect that causes different visual appearance of the material can find use as a humidity sensor in food packaging applications.

Keywords Cellulose acetate · Films · Solution casting · Morphology · Crystallinity · Micropatterning

A. Kramar (✉) · I. Rodríguez Ortega · J. González-Benito
Department of Materials Science and Engineering and Chemical Engineering, Instituto Tecnológico de Química y Materiales "Álvaro Alonso Barba", Universidad Carlos III de Madrid, Avda. Universidad 30, 28911 Leganés, Madrid, Spain
e-mail: akramar@ing.uc3m.es

G. González-Gaitano
Department of Chemistry, Universidad de Navarra, 31080 Pamplona, Navarra, Spain

Introduction

Cellulose acetate (CA) is one of the most important derivatives of cellulose that is recently coming into focus of research for the production of nanofibers and films for food packaging (Espitia et al. 2011; Paunonen 2013; Vartiainen et al. 2014; Do Socorro Rocha Bastos et al. 2016; El Fawal et al. 2019). CA has excellent film forming capabilities; it is chemically and thermally stable, biocompatible and non-toxic. CA can be considered slowly biodegradable or potentially biodegradable (Buchanan et al. 1993; Yadav and Hakkarainen 2021), since it is a derivative of biodegradable cellulose. However, depending on the degree of substitution and environmental conditions, the rate of degradation can be very different (Yadav and Hakkarainen 2021). Its current use

is mostly in textile fibers, filters and eyewear frames (Kamide 2005; Menachem 2007). Current research into the uses of CA films aims, besides at food packaging (Espitia et al. 2011; Vartiainen et al. 2014; Do Socorro Rocha Bastos et al. 2016; El Fawal et al. 2019), at the removal of pollutants from water (De Carvalho Eufrásio Pinto et al. 2019; Gopi et al. 2019), filtration in general (Filho et al. 2005; Vinodhini et al. 2017), elimination of microorganisms from water (Xie and Hung 2019), and preparation of conductive polymer based films by addition of copper (Shivamurthy et al. 2019).

CA is produced by the acetylation of cellulose (conversion of hydroxyl groups of cellulose to acetyl). The full conversion of the hydroxyl groups per anhydroglucose unit produce the so-called, triacetate. In an industrial production of CA, cellulose is firstly converted into triacetate and then hydrolyzed to diacetate to obtain commercial CA with degree of acetylation (substitution of hydroxyl groups by acetyl ones) around 2.5, which significantly affects its solubility. This type of acetate is easily soluble in acetone (Menachem 2007).

The preparation of films using solution casting method of CA in acetone, standalone or mixed with other polymers (Yang et al. 2013) is a simple yet very robust method (Wu et al. 2014; Gonçalves et al. 2019). The usual procedure for polymer casting consists in preparing and pouring the solution on a mold or substrate, followed by the evaporation of the solvent under controlled or partially controlled conditions (Yang et al. 2013; Do Socorro Rocha Bastos et al. 2016; El Fawal et al. 2019; Rodríguez et al. 2019; Yadollahi et al. 2019; Lyytikäinen et al. 2021). However, the influence of environment variables during casting (temperature, humidity or type of casting surface) on the resulting properties of films such as wettability and optical behavior, have been scarcely described in the literature.

It has been reported in several studies that drying conditions can influence the final properties of the films. Recently, Lyytikainen et al. (2021) have shown that drying temperature affects the wetting and barrier properties of films prepared from various cellulose derivatives using solution casting (methyl cellulose, hydroxyethyl cellulose and microfibrilated cellulose). Likewise, the surface roughness of glass Petri dishes used as substrate for casting has proven to induce the formation of air bubbles trapped in the films dried above ambient temperature (50 °C), affecting the morphology and consequently the barrier properties of the films (Lyytikäinen et al. 2021).

Harini and Sukumar (2019) compared open air and vacuum drying conditions (for the preparation of CA films on Petri dishes and found that transparent films were obtained under vacuum, while white films formed in open air drying. An increased order in the surface of the CA films in open air drying conditions caused by a higher crystallinity degree (Harini and Sukumar 2019), was proposed as the most likely cause of the whitish appearance of the films, although the effects of the material of the Petri dishes were not dealt with.

The possibility that drying conditions, as shown by Harini and Sukumar (2019) and Lyytikainen et al. (2021), can influence the appearance of the films, and their optical properties in general, seems very promising, especially in cellulose-based films. A recent research explored the possibility of tuning the optical properties of cellulose films by casting microfibrilated pulp on hydrophilic and hydrophobic surfaces (Mirvakili et al. 2021). Opaque or translucent films were produced by self-assembly of microfibrilated cellulose pulps on the different casting surfaces. The hydrophobic surface of PTFE induced the assembly of microfibers in such way that it yielded convex, translucent films, while a hydrophilic glass surface led to a concave arrangement, producing opaque microfibrilated cellulose films (Mirvakili et al. 2021).

Considering the above mentioned, there is not yet a clear answer about the cause of the optical properties and visual appearance of films induced by the environment casting conditions, as well as the subjacent mechanisms associated to casting conditions. Yet, this knowledge could help to tune the optical properties of the CA films in a very simple way, especially on a large-scale production of CA-based films, which has been the motivation of the present work. In this investigation, the influence of the relative humidity, casting substrate surface used (borosilicate glass, soda-lime glass and micropatterned Teflon-PTFE) and polymer concentration of the solutions of CA have been the variables considered to investigate their effect on the morphology, structure, thermal, and wetting properties of the films.

Materials and methods

Materials

Cellulose acetate, CA (Sigma Aldrich, average Mn ~ 30,000, water content ≤ 3 wt%) was used as received for the preparation of cast films. The degree of substitution, DS, as determined by ATR-FTIR (Fei et al. 2017) is 2.26.

Acetone (Sigma Aldrich, HPLC Plus ≥ 99.9% purity) as solvent and chlorotrimethylsilane (Alfa Aesar, > 98%) as coating agent for soda-lime glass were used as received. Solutions of $MgCl_2$ (Sigma Aldrich, 98% purity), $Mg(NO_3)_2{\cdot}6H_2O$ (Labkem, 99.5% purity) and $CH_3COONa{\cdot}3H_2O$ (Sigma Aldrich, 99% purity) were prepared using distilled water.

Three types of dish were used for casting: borosilicate glass (BS), soda-lime glass (SL) and Teflon (PTFE), purchased from Labbox Labware S.L. Spain, with a diameter of 100 mm.

Casting of films

Solutions of CA, 8%, 10% and 12% (w/v) were prepared by dissolving the polymer powder in the required amount of acetone.

During preliminary experiments, it was observed that, upon drying, CA strongly adhered to the surface of SL Petri dishes. Therefore, chlorotrimethylsilane was used for coating prior to casting the solutions. We applied the coating 10 min before casting by pouring ca. 0.2 ml of chlorotrimethylsilane on the center of the glass Petri dish and spreading it all over the surface using a silicone brush. According to the best of authors' knowledge, there is not any optimized procedure described in the literature.

A set of solutions were first cast in open air (OA, hereafter) at temperature 22 ± 2 °C and 35 ± 5% relative humidity (RH) on circular dishes made of borosilicate glass (BS), soda-lime glass (SL) and PTFE by depositing 0.1 ml cm^{-2} of solution. On the other hand, the same set of solutions was also cast placing the dishes in a perforated box (Fig. 1), fixing the humidity at least 24 h prior to casting to ensure its' stabilization, which was controlled in the box with a saturated saline solution ($MgCl_2$ for 35% RH; $Mg(NO_3)_2 \cdot 6H_2O$ for 55%; and $CH_3COONa \cdot 3H_2O$ for 75%). The temperature during casting was 22 ± 2 °C, the same as under OA conditions. The holes on the side of the box favored the removal of the solvent from the casting chamber, keeping the desired humidity. Films were left in the box until complete evaporation of the solvent for 24 h and then detached from the surface and stored in aluminum foil for further analysis.

Characterization of the films

The samples morphology was investigated using an optical profilometer Olympus DSX500 (Olympus Iberia, Barcelona, Spain). Roughness parameters were obtained according to the standard EN ISO 4288 (1997), specifically R_a(arithmetic mean roughness), over a sample area of 1499 × 1499 µm. An average value was taken from six linear profiles (3 in the X direction and 3 in the Y direction). Samples were tested on the up side (in contact with air)

Fig. 1 Perforated box (red arrows) used to keep constant the relative humidity during the casting of CA films

and on the down side (in contact with the casting surface). The cut-off wavelength, λ_c, used to carry out the fits in the roughness analysis, was selected according to standard EN ISO 4288.

Films thickness was measured with a portable Easy-check FN (Neurtek Instruments) coating thickness meter, with an accuracy of ± 1 µm, and given as an average of 20 measurements per sample (2 × 10 measurements per film).

The transparency of films was measured using a Jasco V650 UV–VIS spectrophotometer. Films were cut in a rectangular shape (approx. 1 cm × 2 cm) and transferred to the cell holder, while the baseline was recorded without any sample. Transmittance and absorbance were measured in the 400–700 nm range, while the transparency was calculated by dividing the absorbance at 600 nm by the film thickness, according to described methodology (Tee et al. 2016; Sukhija et al. 2018). Film thickness used for a transparency value calculation, is an average of 5 measurements directly performed on the samples used for UV–VIS.

Wettability was evaluated by measuring the contact angle between distilled water and the CA films using an OCA-15 Plus Goniometer (Data Physics, Neurtek Instruments, Eibar, Spain) and following the sessile drop method. The contact angles were the average of 4 measurements per each side of the specimens. In order to evaluate the evolution of wetting, snapshots of the water drops (3 µl volume) on the surfaces of the materials were taken as a function of time up to 300 s, measuring at each time the corresponding contact angles.

Attenuated total reflectance Fourier transformed infrared spectroscopy, ATR-FTIR, spectra were recorded on a Shimadzu IRAffinity-1S spectrometer equipped with a Golden Gate ATR accessory (diamond window), from 600 to 4000 cm^{-1} with a resolution of 4 cm^{-1} and averaging 32 scans. Each sample was measured twice at different locations on both sides of the films. The spectra were analyzed using KnowItAll Spectroscopy software (Academic edition, Willey Science Solutions). The determination of the degree of substitution of CA acetate, *DS*, was determined from the analysis of the spectra according to (Fei et al. 2017), as

$$DS_{C=O,A} = 1.4301 + 0.2841r + 1.5502r^2 \quad (1)$$

where r is the ratio between the peak areas of the carbonyl stretching band of the acetyl group (1737 cm^{-1}) and the cellulose backbone (1033 cm^{-1}).

XRD diffractograms were recorded with an X-ray powder diffractometer Bruker ECO D8 Advance (Bruker, Karslruhe, Germany), using the Cu-K_{a1}, λ = 1.5418 Å. Samples were placed on an amorphous glass holder and the diffractograms recorded from 10° to 40° in 2θ at 2 s per step with 0.02° of step size. Samples for both XRD and FTIR tests were measured under ambient temperature and humidity conditions.

Peak fitting was carried out with PeakFit software, using the minimum possible number of peaks for obtaining the best fit (R^2 resulted ≥ 0.97 in all samples). Peaks for deconvolution were chosen from the diffractogram of the powder CA and following the literature peak assignation. Crystallinity index was calculated by dividing the sum of the peak areas corresponding to crystalline planes in the diffractogram by the total area (Park et al. 2010; Karimi and Taherzadeh 2016; De Freitas et al. 2017; Ivanovska et al. 2019).

Thermal behavior of the cast films was studied by differential scanning calorimetry, DSC, using a Mettler Toledo 822e calorimeter, under nitrogen atmosphere. Samples (4.5–5 mg) were subjected to the following thermal cycles: (a) first heating scan, 50–300 °C at 10 °C/min; (b) isothermal step at 300 °C for 5 min; (c) cooling scan, 300–50 °C at 10 °C/min; (d) second heating scan, 50–300 °C at 10 °C/min. The crystalline fraction of the cast materials, χ, was calculated from the first heating cycle by dividing the enthalpy of fusion of the samples by 58.8 $J \cdot g^{-1}$ (the enthalpy of triacetate cellulose 100% crystalline, Cerqueira et al. 2006).

Results and discussion

Influence of casting conditions on morphology of CA films

The controlled evaporation of the solvent of the CA solution was found to be a crucial factor regarding the general appearance of the dried films. Thus, films cast on glass in OA showed much higher unevenness and defects (Fig. 2) compared to those cast under controlled humidity. Unevenness of the films cast in OA is probably due to the non-controlled air flow over the

films when drying, which leads to a faster evaporation rate. As can be seen in Fig. 2, the OA-cast films were not smooth, showing a wrinkled surface. However, those cast under controlled humidity showed much smoother appearance, although with slightly lower transparency as humidity increases (Fig. 2 and Table 1).

As can be seen from the values in Table 1, transparency decreases when humidity increases, while the lowest transparency is observed in films cast on PTFE. Transmittance values of these films are even different when the two sides are compared, upper side (side in contact with air during drying) yielding a slightly lower transmittance.

When the films are observed with the optical profilometer, interesting features can be noticed (Fig. 3). The surface of the films directly in contact with PTFE showed in all cases a very distinctive pattern, in the form of circular channels, regardless of polymer concentration used. Additionally, the films cast on PTFE showed a pattern on the downside (i.e. in contact with the dish) but were flat on the side in contact with air, which exhibited a glossy appearance.

The pattern imprinted into the films by the topography of the PTFE surface can scatter light, producing the translucent appearance. The dimensions of the circular channels observed in the films cast on PTFE were 40.6 µm ± 1.5 µm in width and 1.2 ± 0.4 µm in depth (average of 10 measurements). Since the depth of these channels is ca. 1 µm and they present a concave shape, their dimensions are comparable to the wavelength of visible light, which is the reason for the scattering of light and opacity.

Table 1 Light transmittance, absorbance and transparency value at 600 nm for differently cast CA films from solutions in acetone (10% of CA)

Sample	Transmittance %	Absorbance	Transparency value
35%	91.7	0.38	5.4
55%	89.5	0.49	6.3
75%	89	0.55	8.1
PTFE OA (downside)	21.3	0.67	11.2
PTFE OA (upper side)	17.6	0.75	12.5
PTFE-55 (downside)	30	0.52	10.4
PTFE-55 (upper side)	29.8	0.52	10.4

The OA-cast films on glass dish at 35% RH exhibited a hexagonal-like pattern (Fig. 4) throughout the sample generated by the accumulation of material at the hexagon edges, and most likely due to a surface tension effect induced by the fast evaporation rate that occurs when the relative humidity is low enough and air currents are present. When PTFE dish is used in OA evaporation conditions, the same hexagonal pattern could also be observed on the upper side of the film, which suggests that the film topography is not induced by the morphology of the PTFE surface. It can be concluded that hexagonal-like pattern is a consequence of the drying forces at lower humidity, possibly related to evaporation rate of the acetone, rather than to the topography of the dish surface.

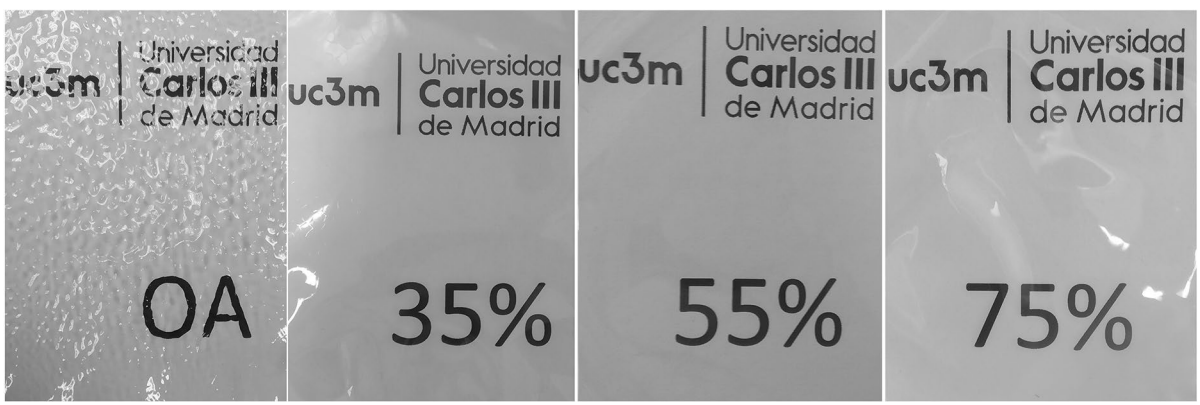

Fig. 2 Visual appearance of films prepared by solution casting method in open air (OA) and at different humidity (35%, 55% and 75% RH) from a 10% CA solution in acetone

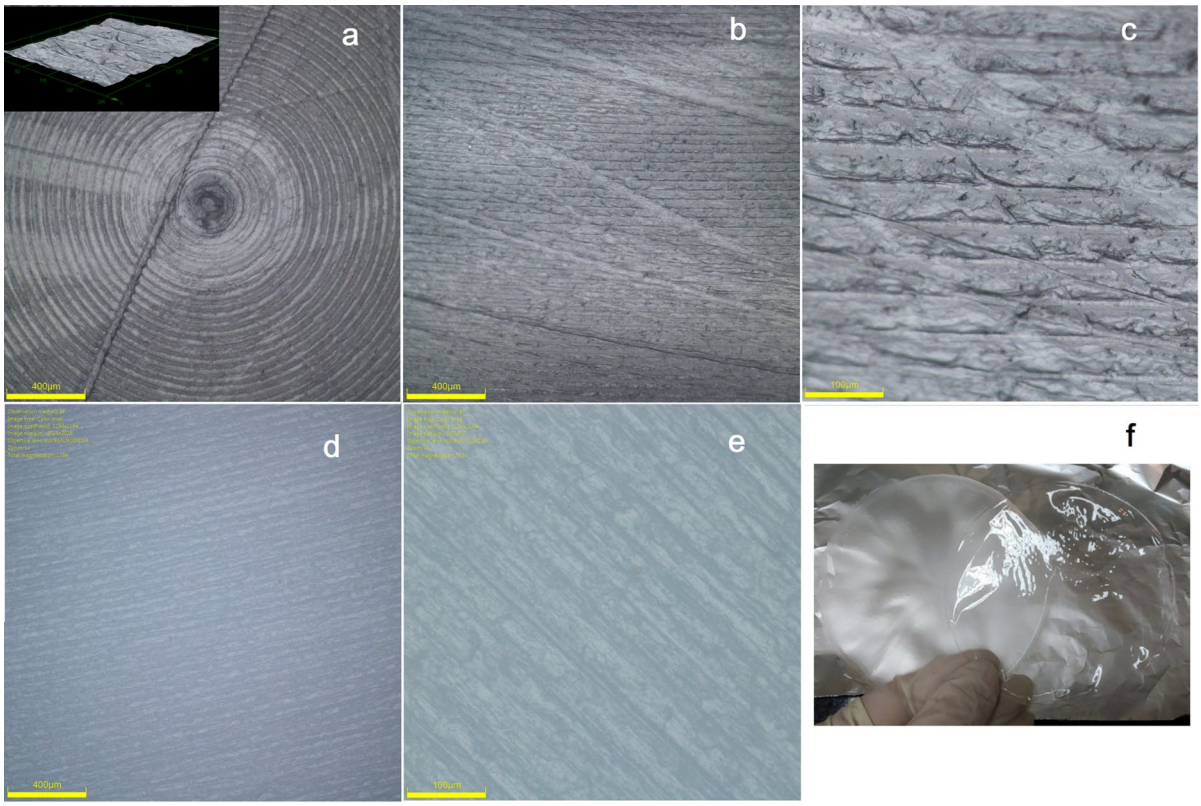

Fig. 3 CA film cast from a 12% solution in acetone on a patterned PTFE dish. **a** Center of the film surface in contact with the dish; inset of a 3D image at higher magnification; **b** film surface far apart from the center of the film; **c** higher magnification of the region in image **b**; **d** surface of PTFE dish at the same magnification as in **b**; **e** surface of PTFE dish at the same magnification as **c**; **f** visual appearance of films cast on PTFE (translucent) and flat glass (transparent), respectively

Under controlled atmosphere casting, the rate of solvent evaporation is slower. At low humidity (35% RH) some defects, similar to those present in OA-cast films (at the same humidity) could be seen but, in general, they appear more uniform and flat. Increasing the humidity up to 55% led to the disappearance of these patterns on the upper side of the films. It seems therefore that the morphological features observed in OA films are a consequence of the low humidity environment and fast evaporation rate. Under higher humidity, even though the temperature remains constant, the solvent evaporates more slowly due to the saturated humid air above the surface. At 75% RH, some defects in the form of trapped air bubbles can be seen (Fig. 4), although flatness is preserved, with no large defects, and with a whitish appearance (Fig. 2). Considering that an increase in the crystallinity scatter light (Harini and Sukumar 2019) and causes the opaque appearance of the material, the crystallinity was further studied (as shown in the following section).

Roughness of the films (Fig. 5) was found to be independent on the polymer concentration of the solutions, without significant differences between the upper and down sides, except for the samples cast from 8 and 10% CA, at 35% RH. Furthermore, the standard deviations for the roughness parameters were higher for the films prepared at 35% RH and decreased when increasing the humidity, suggesting that the film heterogeneity increases, despite the similar roughness.

There is not a clear trend of the roughness as a function of humidity during casting but differences can be observed with the casting dish type. Thus, regardless the concentration and for a 55% RH, CA films cast on PTFE presented 48% lower average roughness (R_a) in both upper and down sides compared with glass cast films, which can be ascribed

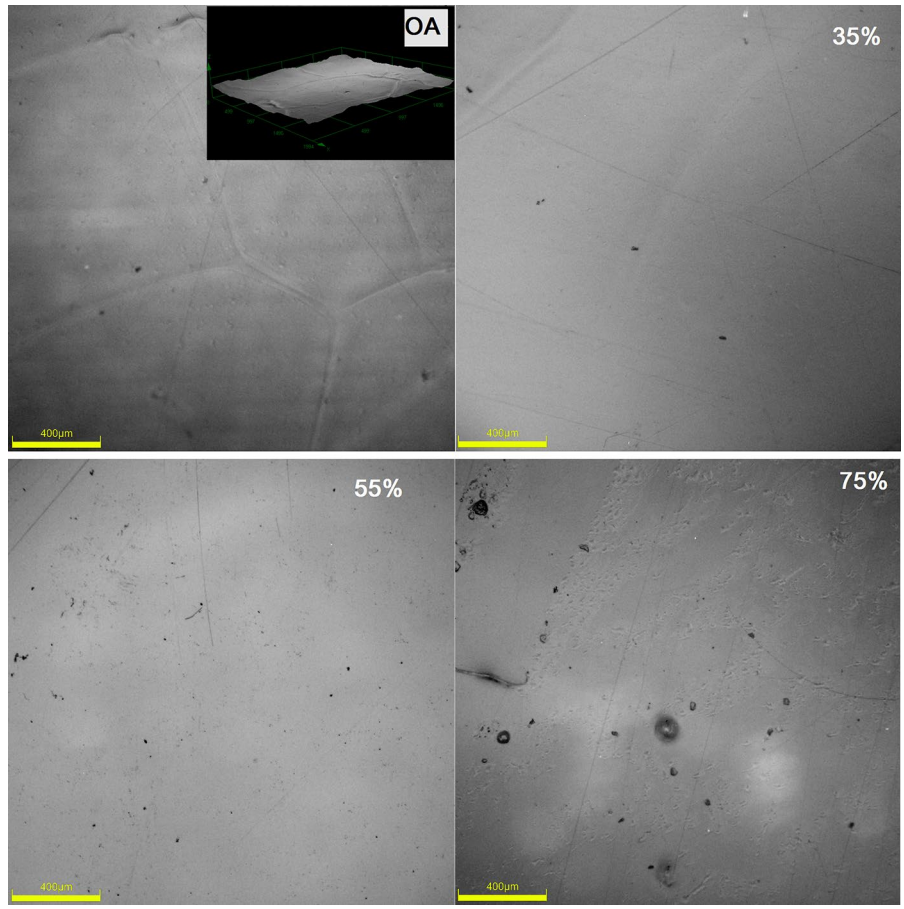

Fig. 4 CA film cast on a coated soda lime glass surface in open air (OA) from an 8% acetone solution in open air and at different humidity conditions (35%, 55%, 75% RH)

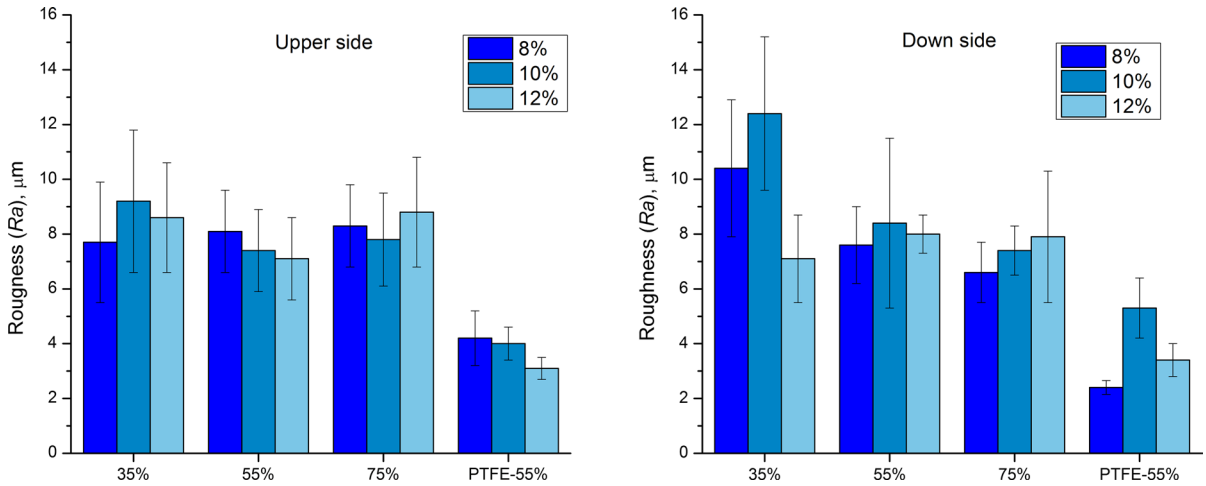

Fig. 5 Roughness parameter (R_a) measured on both sides of films cast on glass at different humidity or on PTFE at 55% RH, as a function of CA concentration (8%, 10% and 12%)

to variations in the evaporation rate depending on the nature of the substrate used for casting. When a glass dish is used instead, the films are more easily detached from the surface compared to the ones cast on PTFE. From roughness results it can be concluded that the average roughness (R_a) of films depends on several factors, including casting conditions specifically humidity, type of surface substrate used for casting and concentration of the polymer all of them affecting the drying kinetics, while the dominant factor influencing the roughness cannot be determined.

Thickness of films was used for calculating the transparency values but also to study the thickness variation with different casting conditions. As expected, the thickness of the films increased with the polymer concentration (Table S1 Supplementary material). The data dispersion also increased with the concentration of CA, which can be explained by the fact that increasing viscosity of polymer solution leads to to unevenness in the cast film. Interestingly, thinner films are obtained on PTFE under the same conditions, i.e. using the same concentration. This can be related also to the fact that, when films were cast on PTFE, they needed to be peeled off from the surface while those cast on glass were completely detached from the surface. This indicates a certain shrinkage of the glass-cast films, which causes them to be slightly thicker than PTFE-cast films.

Influence of casting conditions on the structural properties of films

The effect of the casting conditions on the films structure was studied by ATR-FTIR spectroscopy and XRD. The films obtained from 10% polymer solutions were considered as representative ones and their FTIR spectra are presented in Fig. 6.

In each case, the typical absorption bands of CA were observed. The broad band around 3400 cm^{-1} is assigned to non-esterified hydroxyl groups of cellulose, while the weak band at 2945 cm^{-1} corresponds to the CH antisymmetric stretching of the CH_3, which is slightly shifted to 2949 cm^{-1} in the case of the film cast at 75% RH, along with the weak band at 2886 cm^{-1} that corresponds to the CH_3 symmetric stretching. The strong absorption at 1737 cm^{-1} corresponds to the carbonyl group stretching, which does not change under the processing conditions used to cast the films. The signal at 1369 cm^{-1} corresponds to the symmetric CH_3 bending band, and the antisymmetric C–O–C stretching mode appears at 1219 cm^{-1} and 1033 cm^{-1}, respectively (Gonçalves et al. 2019; Figueiredo et al. 2020). The acetylation degree of the cellulose can be obtained from the ratio between the areas of the carbonyl stretching (1737 cm^{-1}) and the C–O–C stretching (1033 cm^{-1}) (Fei et al. 2017), resulting in a *DS* value of 2.26. The bands at

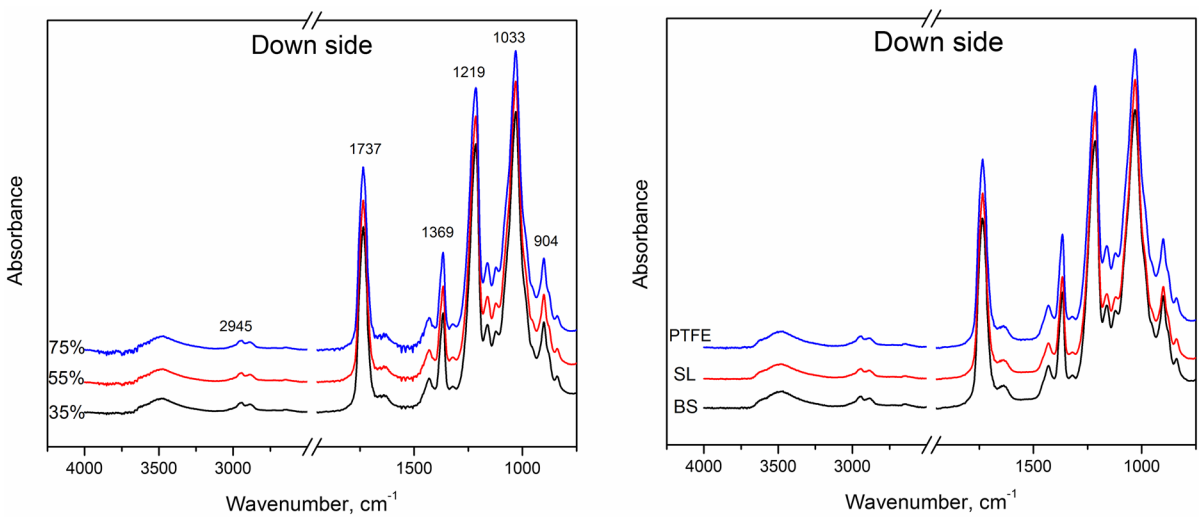

Fig. 6 ATR-FTIR spectra of cast CA films (down side) at various humidity conditions (35%, 55%, 75% RH) on glass (left), and on different surfaces (right) in open air, OA (PTFE-Teflon, SL-soda lime glass coated with chlorotrimethylsilane, BS-borosilicate glass)

1430 cm^{-1}, 1369 cm^{-1}, 1162 cm^{-1} and 895 cm^{-1} are characteristic for the cellulose I structure (Carrillo et al. 2004), from which CA is obtained by acetylation. Finally, the characteristic peak at 904 cm^{-1} is assigned to acetate methyl groups. Overall, it can be concluded that the nature of the dish to carry out the casting has no effects on the structure at a microscopic level of the films, irrespectively of the film side. Likewise, the relative areas of the 3000–3800 cm^{-1} region (stretching vibration of the –OH groups of cellulose) are virtually the same for all the samples, as an indication that there is no presence of adsorbed water due to the different humidity conditions used during casting.

The films structure has been also tested by XRD, in order to detect any variations in the crystallinity of the materials. Figure 7 shows the diffraction patterns for the films prepared under different conditions.

As can be seen, the powder CA diffractogram can be resolved into four sharp peaks, at 10.6°, 13.4°, 22.3°, and 34°. The last two ones can be assigned to cellulose I_β diffraction planes 200 and 004, respectively (Fan et al. 2013). Peaks at 10.6° and 13.4° have been reported as typical for semicrystalline CA, i.e. crystalline peaks of CTA II polymorph (Fan et al. 2013; Chen et al. 2016; De Freitas et al. 2017; Gonçalves et al. 2019). On the other hand, the broad diffraction at 18.2° and 21.4° is due to amorphous cellulose (Park et al. 2010; Das et al. 2014).

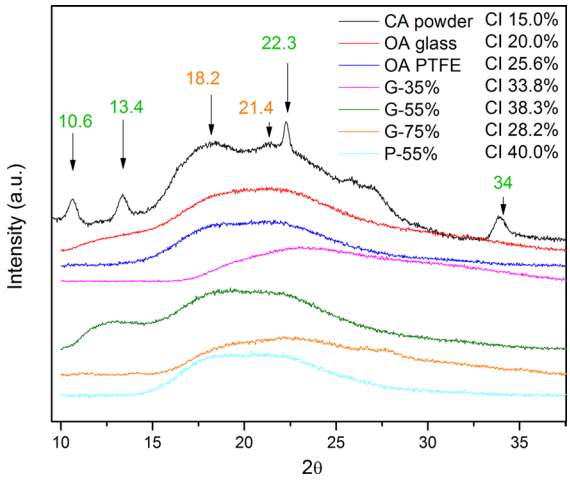

Fig. 7 XRD spectra and crystallinity index (CI) of cast CA films under various humidity conditions (OA-open air, 35%, 55%, 75% RH) and on different surfaces (PTFE-Teflon, G-soda lime glass coated with chlorotrimethylsilane)

Variations in the XRD pattern between films produced under different casting conditions can be observed. The peaks at 10.6° and 13.4° disappear, with the exception of the films cast on SL glass at 55% and 75% RH. In the first case, a broad band in the region from 10° to 14° can be deconvoluted to a single peak at 13.0°. In the second case, two barely observable peaks at 12° and 14° appear. The crystallinity is in the range from 20 to 40%, depending on the conditions used for casting (Fig. 7). According to the XRD data, the lowest crystallinity corresponds to the film cast in OA on SL glass, while the highest is for films cast under 55% RH on both glass and PTFE. Regardless of the surface used for casting, higher humidity combined with controlled evaporation in a closed environment generates more crystalline films. In a closed environment at higher humidity, the solvent evaporates more slowly, which permits the polymer chains to reorganize into more ordered structures. The results obtained in our study are comparable to other findings in the literature (De Freitas et al. 2017), using CA of DS 2.29, nearly similar to the one used in our study.

Although XRD is a powerful technique for studying the crystallinity of polymers, the strong contribution of the amorphous halo to the diffractogram can make the calculation of this parameter less precise (Park et al. 2010; Karimi and Taherzadeh 2016). Due to this, DSC has been used to additionally calculate this parameter, along with the thermal properties of the films (Wan Daud and Djuned 2015; De Freitas et al. 2017; Gonçalves et al. 2019).

Regarding the thermal behavior of the cast films the observed thermal transitions match those reported in the literature, as expected (Kamide and Saito 1985; Kennedy et al. 1995; Zugenmaier 2004). Melting temperatures from the first heating scan ranged from 226 to 233 °C (Fig. 8), in accordance with the wide range of melting temperatures reported for CA (from 220 to 300 °C), depending on the degree of acetylation and source of cellulose (Barud et al. 2008; Wan Daud and Djuned 2015; Yadollahi et al. 2019). However, the glass transition temperature, T_g, was not detected in any of the films in the first heating scan, in contrast to what was reported for some commercial samples of CA (Zugenmaier 2004; Kamide 2005). Along the first heating scan in this investigation, the T_g was only clearly observed in the case of the film prepared on glass in OA, at 195 ± 2 °C, a value similar to the one

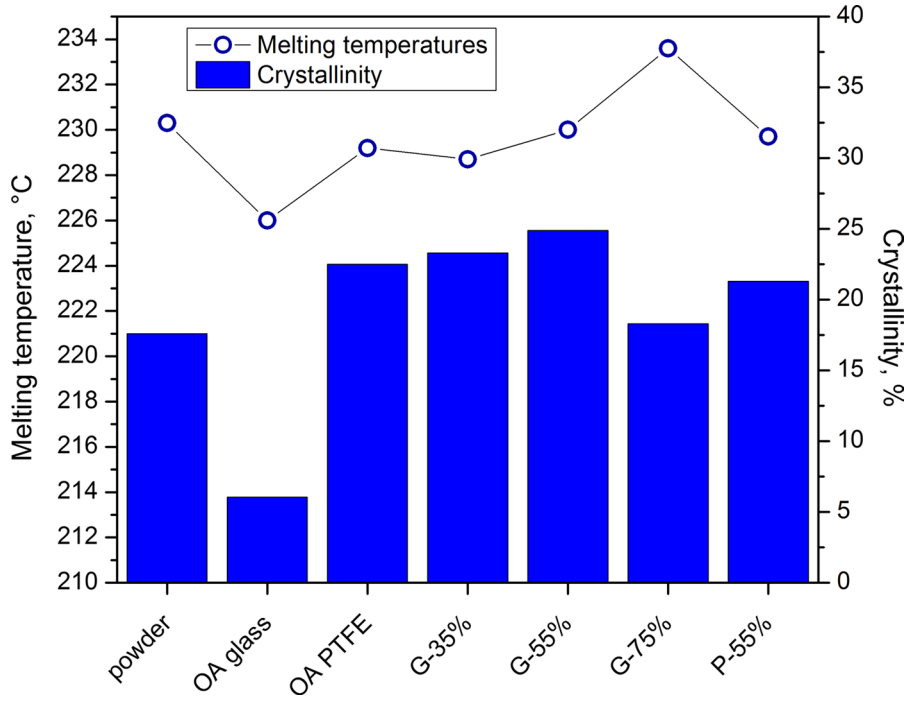

Fig. 8 Crystallinity and peak melting temperatures obtained from DSC of CA films prepared in open air (OA) at different RH from 10% solutions in acetone

reported by (Zugenmaier 2004). The second heating scan reveals a very distinctive T_g in all samples in the 180–200 °C range (data not shown) and small enthalpies of fusion, between 210 and 220 °C, confirming that CA cannot recrystallize to the same extent by heating and cooling cycles, but evidently can crystallize from an acetone solution after casting; similarly, the inability od secondary cellulose esters to recrystallize by melting, has been proposed by Boy et al. (1967).

Casting under different conditions led to changes in melting enthalpy and, therefore, crystallinity (Fig. 8). As can be seen, the film with the lowest crystallinity is the one cast on glass in OA which, in turn, shows the lowest T_g. Therefore, it could be that crystallinity is the main cause of the presence or absence of T_g in the first heating scan. High crystallinity degree may make the detection of T_g more difficult because of low DSC sensitivity and possible overlapping of the endotherm glass transition and melting signals, which are in close temperature range in cellulose acetate. The crystallinity can be related to the evaporation rate of the solvent during drying. When films are cast in OA, the uncontrolled airflow above the solution causes faster evaporation and less time for the polymer chains to organize, which would justify the lowest crystallinity found in films cast in OA. Additionally, by comparing films cast in OA on different surfaces we can conclude that increased order is present in CA cast on PTFE surface, compared to the materials cast on glass, which had the lowest melting enthalpy of all analyzed samples, even lower than the initial powder CA. This is in accordance with the results obtained by Liu and Lo (2002) where a lower value of the enthalpy of fusion was measured using DSC for cast CA compared to powder polymer.

In our work, DSC crystallinity results partially corroborate the XRD findings. A general trend of crystallinity increase with the humidity up to 55% RH is observed from both methods, as well as a decrease of crystallinity in the sample cast at 75% RH. Even though crystallinity decreased, transparency decreased as well (Table 1), despite the expected effect that higher crystallinity can cause lower transparency in polymeric films (Harini and Sukumar 2019).

In this particular case, the transparency decrease can be explained considering a phase separation process. Evaporation, when the humidity is high enough, may lead to phase separation since water is a precipitant for CA dissolved in acetone. Therefore, a certain extent of phase separation on the

upper side of the films (the one directly in contact with moisture) is to be expected. In order to corroborate this, a 10% CA solution in acetone was cast at 90% RH, which resulted in white spots all over the surface of the film (Fig. 9).

Similarly, the translucent optical appearance of PTFE cast films can be explained as a consequence of changes in morphology rather than in crystallinity. The results of crystallinity point out as the only explanation of the different optical behavior, that the surface patterns generated in the film depend on the substrate surface used to carry out the casting. As it was seen in the optical images, the patterned surface of film, more precisely the side of the film in contact with the dish, adopted the pattern from the PTFE, which causes scattering of light similar to the so-called etched glass. Etching of the glass creates nano and microroughness that can cause transmitted light to scatter and produce various optical effects (Fouckhardt et al. 2007). High surface roughness, according to other researches, enhances surface hydrophobicity, and additionally modifies the transparency to translucent or opaque due to light scattering effect (Chen et al. 2018; Liu et al. 2021).

Therefore, in terms of desired high transparency, and considering the results on the morphology and crystallinity, the most optimal conditions for film casting would be 55% RH in a closed chamber using SL glass dishes coated with chlorotrimethylsilane. These conditions produce different effects: (1) slow down the evaporation rate; (2) reduce the possibility of turbulent air flow during drying; and (3) reduce the heterogeneity of the film surface, which can affect the morphology, optical appearance and thermal properties of films. On the other hand, for applications that require semitransparent films, a simple patterned mold or dish can be used to induce translucency, which will be independent of humidity conditions during casting.

In summary, we presented that casting conditions clearly influence the properties of films; therefore, we propose that in the preparation of polymeric films by casting, and especially CA, precisely defined conditions should be used and reported.

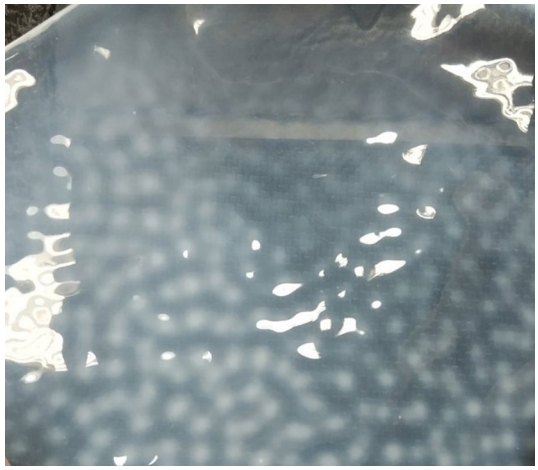

Fig. 9 Appearance of a CA film cast at 90% RH

Wettability and optical tunability upon wetting of films

CA is less hydrophilic than cellulose due to acetylation. However, acetate films are not properly hydrophobic and their contact angle is usually lower than 90°, as reported for solution cast (Wu et al. 2014) or spin-coated thin CA films (Mikaeili and Gouma 2018).

The static contact angle using the sessile drop method was measured on both sides of films cast on glass and PTFE (Figs. 10 and 11). The results indicate hydrophilic nature of cast cellulose acetate films since measured contact angles are lower than 90°. While there is no clear correlation between humidity during casting and wettability of the films (Fig. 10), a clear influence of the patterned surface of PTFE film on wettability (Fig. 11) can be noticed (representative snapshots of water drops on the films obtained during contact angle measurements are given in Supplementary material).

The wettability tests were performed up to 5 min upon contact of water on the surface. In all samples, a small reduction of the contact angle over time (up to 10% of the initial value in the first 5 min of water contact).

In general, the highest contact angle was obtained for films cast on PTFE in OA, without humidity control. Higher wettability (lower water contact angle) was obtained in samples cast on PTFE at 55% RH compared to the same sample cast in OA (Fig. 11). As expected, the lowest wettability was detected on patterned PTFE dish (Fig. 11). When

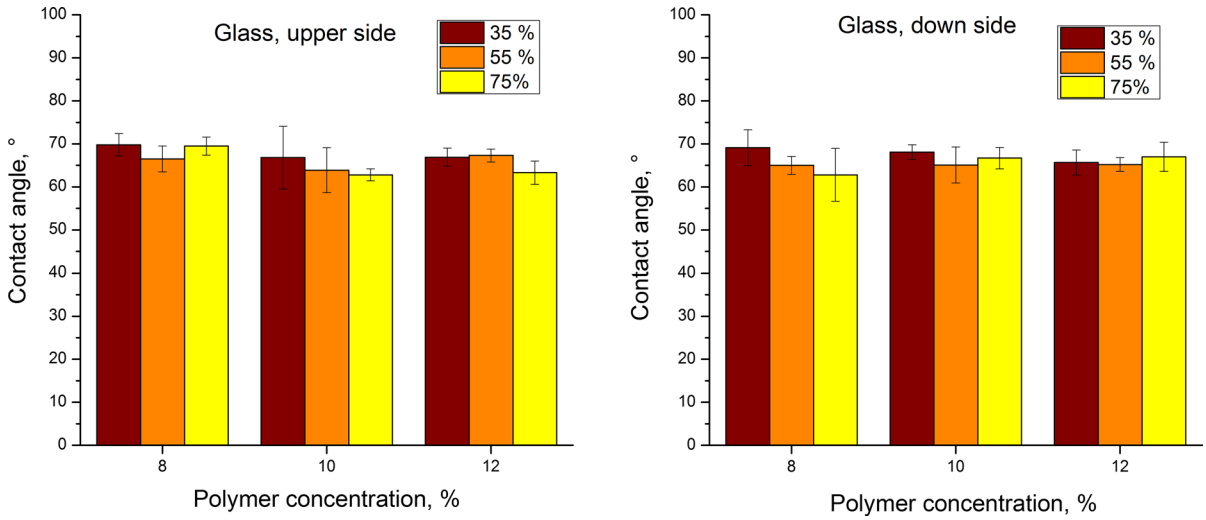

Fig. 10 Contact angle values on upper and down sides of films cast on soda-lime (SL) coated glass at 35%, 55% and 75% RH

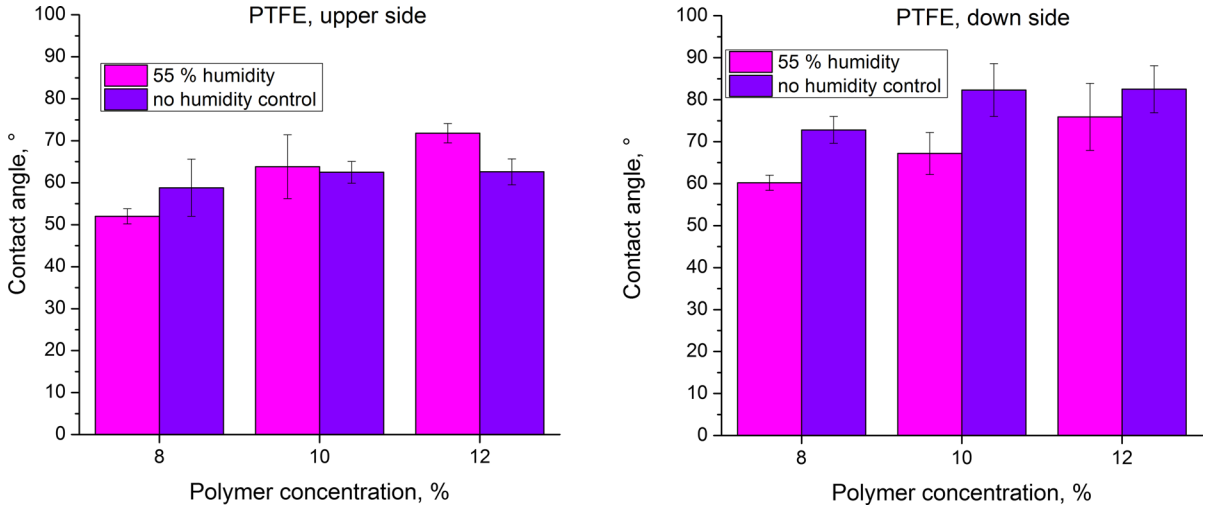

Fig. 11 Contact angle values of upper and down sides of films cast on PTFE surface at controlled humidity (55% RH) and in open air (OA, no humidity or air flow control)

observing the contact angles on both sides of films cast on glass, the differences are within the experimental error compared to films cast under controlled humidity. However, when there is no control of this variable (as in OA conditions) significant differences appear when comparing different sides of the films. As can be seen from Fig. 11, for films cast on PTFE, the contact angle of patterned down side is 32% higher than that of the upper side. It is usually admitted that rough surfaces tend to lower the wettability (Hansson et al. 2011; Dimic-Misic et al. 2021). In the present work, the mere change in roughness is not the main reason for a change in wettability, but rather the patterned surface with regular periodic morphology, causes the higher contact angle. Even though samples cast on glass dishes have higher values of R_a (Fig. 5), their wettability is higher, compared with the patterned surface of the film cast on PTFE (down side). Hence, when considering wettability and roughness, not just the

R_a should be taken into account but periodicity originating from micropatterns on the surface, as well.

Moreover, an interesting effect was noticed in the case of samples cast on PTFE. The patterned side, when wetted, becomes transparent, a result that was also confirmed using optical microscopy (Fig. 12). Upon wetting, the film surface is more even due to the fact that water (with similar diffraction index as the film) fills the groves on the surface, rendering the film transparent. This optical effect is fully reversible: water can be removed from the surface by simple wiping and the translucency is recovered. This also confirms that the higher contact angle in films prepared with a patterned surface is not a consequence of trapped air, as it would be if wettability follows the Cassie–Baxter regime of wetting (Hansson et al. 2011), but it rather follows the Wenzel regime, where water wets the extra area of channels present in the films, which are themselves rough and not smooth as seen by optical microscopy.

Thus, the films prepared in this work, specifically those obtained on a PTFE surface, can have potential applications in active food packaging, as they become transparent when wetted. This could prove useful as a moisture indicator for example, by using a tunable translucent side as the inner side of food packaging. The micropatterning produced during casting, using a controlled topography of the substrate, can be further explored to obtain other optical effects. Tunable optical effects induced by micropatterning can be used to design sensors in active food packaging application (Mustafa and Andreescu 2018), avoiding for instance addition of chemical and biological additives.

Conclusions

Preparation of cellulose acetate (CA) films using solution casting method was performed using different surfaces (borosilicate glass, soda-lime glass and PTFE) and under different humidity conditions. It was found that casting under controlled humidity and in an environment of slower evaporation rate of the solvent leads to a higher film crystallinity, increased transparency and more homogeneous appearance. The most optimal conditions were found to be at 55% RH where cast films have the optimal transparency, smooth appearance without defects. CA films cast on micropatterned PTFE surface exhibited optical anisotropy as the film side directly in contact with the PTFE adopted its patterned microstructure. The resulting films were translucent but they became transparent when the

Fig. 12 Macroscopic (top) appearance of CA patterned films obtained on PTFE surface, in dry (left) and wet (right) state and microphotograph of corresponding surfaces (bottom); circular translucent film with wetted central part showing difference in transparency

patterned side was wetted. This result opens up a possibility for producing polymeric CA films with tunable transparency in a straightforward manner, by simply changing their morphology with an adequate selection of a patterned casting surface.

Ambient conditions, such as humidity, can thus affect the transparency, wettability and uniformity of the CA films. Likewise, although a partial control of the solvent evaporation was achieved in this work, more studies on the kinetics of evaporation and its relation to the resulting film properties are necessary, which are the objective of a further study. As highlighted in this article, we propose that in the future works which involve casting of polymeric films from a solution, precise environmental conditions be used and reported.

Acknowledgments This work was financially supported by CONEX-Plus program of Universidad Carlos III de Madrid (UC3M) and the European Commission through the Marie-Sklodowska Curie COFUND Action (Grant Agreement No 801538). Authors also appreciate the financial support received from AEI (Ministerio de Ciencia e Innovación of Spain, PID2020-112713RB-C22 and -C21); the Universidad Carlos III de Madrid, Fondos de Investigación of Fco. Javier González Benito (2012/00130/004) and the strategic Action in Multifunctional Nanocomposite Materials (2011/00287/003).

Author contributions Conceptualization [AK, JG-B]; Methodology, Investigation, Formal analysis, Validation [AK, IRO, GG-G, JG-B]; Writing-original draft [AK]; Writing—Review and Editing [IRO, GG-G, JG-B]; Supervision [JG-B].

Funding Open Access funding provided thanks to the CRUE-CSIC agreement with Springer Nature. This work was financially supported by CONEX-Plus program of Universidad Carlos III de Madrid (UC3M) and the European Commission through the Marie-Sklodowska Curie COFUND Action (Grant Agreement No 801538). Authors also appreciate the financial support received from AEI (Ministerio de Ciencia e Innovación of Spain, PID2020-112713RB-C22 and -C21); the Universidad Carlos III de Madrid, Fondos de Investigación of Fco. Javier González Benito (2012/00130/004) and the strategic Action in Multifunctional Nanocomposite Materials (2011/00287/003).

Data availability Not applicable.

Code availability Not applicable.

Declarations

Conflict of interest The authors have no relevant financial or non-financial interests to disclose.

Consent to participate Not applicable.

Consent for publication Not applicable.

Ethical approval and ethical standards Not applicable.

References

Barud HS, Araujo Junior AM, De SDB et al (2008) Thermal behavior of cellulose acetate produced from homogeneous acetylation of bacterial cellulose. Thermochim Acta 471:61–69. https://doi.org/10.1016/j.tca.2008.02.009

Boy RE Jr, Schulken RM Jr, Tamblyn JW (1967) Crystallinity in secondary cellulose esters. J Appl Polym Sci 11:2453–2465

Buchanan CM, Gardner RM, Komarek RJ (1993) Aerobic biodegradation of cellulose acetate. J Appl Polym Sci 47:1709–1719. https://doi.org/10.1002/app.1993.070471001

Carrillo F, Colom X, Suñol JJ, Saurina J (2004) Structural FTIR analysis and thermal characterisation of lyocell and viscose-type fibres. Eur Polym J 40:2229–2234. https://doi.org/10.1016/j.eurpolymj.2004.05.003

Cerqueira DA, Filho GR, Assunção RMN (2006) A new value for the heat of fusion of a perfect crystal of cellulose acetate. Polym Bull 56:475–484. https://doi.org/10.1007/s00289-006-0511-9

Chen J, Xu J, Wang K et al (2016) Cellulose acetate fibers prepared from different raw materials with rapid synthesis method. Carbohydr Polym 137:685–692

Chen Z, Li G, Wang L et al (2018) A strategy for constructing superhydrophobic multilayer coatings with self-cleaning properties and mechanical durability based on the anchoring effect of organopolysilazane. Mater Des 141:37–47. https://doi.org/10.1016/j.matdes.2017.12.034

Das AM, Ali AA, Hazarika MP (2014) Synthesis and characterization of cellulose acetate from rice husk: eco-friendly condition. Carbohydr Polym 112:342–349. https://doi.org/10.1016/j.carbpol.2014.06.006

De Carvalho Eufrásio Pinto M, David Da Silva D, Amorim Gomes AL et al (2019) Film based on magnesium impregnated biochar/cellulose acetate for phosphorus adsorption from aqueous solution. RSC Adv 9:5620–5627. https://doi.org/10.1039/c8ra06655h

De Freitas RRM, Senna AM, Botaro VR (2017) Influence of degree of substitution on thermal dynamic mechanical and physicochemical properties of cellulose acetate. Ind Crop Prod 109:452–458. https://doi.org/10.1016/j.indcrop.2017.08.062

Dimic-Misic K, Kostic MM, Bratislav O et al (2021) Iso- and anisotropic etching of micro nanofibrillated cellulose films by sequential oxygen and nitrogen gas plasma exposure for tunable wettability on crystalline and amorphous regions. Materials (basel) 14:3571

Do Socorro Rocha Bastos M, Da Silva Laurentino L, Canuto KM et al (2016) Physical and mechanical testing of essential oil-embedded cellulose ester films. Polym Test 49:156–161. https://doi.org/10.1016/j.polymertesting.2015.11.006

El Fawal GF, Omer AM, Tamer TM (2019) Evaluation of antimicrobial and antioxidant activities for cellulose acetate films incorporated with Rosemary and Aloe Vera essential oils. J Food Sci Technol 56:1510–1518. https://doi.org/10.1007/s13197-019-03642-8

Espitia PJP, Soares NDFF, Botti LCM, Silva WA (2011) Effect of essential oils in the properties of cellulosic active packaging. Macromol Symp 299–300:199–205. https://doi.org/10.1002/masy.200900124

Fan G, Wang M, Liao C et al (2013) Isolation of cellulose from rice straw and its conversion into cellulose acetate catalyzed by phosphotungstic acid. Carbohydr Polym 94:71–76. https://doi.org/10.1016/j.carbpol.2013.01.073

Fei P, Liao L, Cheng B, Song J (2017) Quantitative analysis of cellulose acetate with a high degree of substitution by FTIR and its application. Anal Methods 9:6194–6201. https://doi.org/10.1039/c7ay02165h

Figueiredo AS, Garcia AR, Minhalma M et al (2020) The ultrafiltration performance of cellulose acetate asymmetric membranes: A new perspective on the correlation with the infrared spectra. J Membr Sci Res 6:70–80. https://doi.org/10.22079/JMSR.2019.110424.1269

Filho GR, Chagas Da Silva R, Meireles CDS et al (2005) Water flux through blends from waste materials: cellulose acetate (from sugar cane bagasse) with polystyrene (from plastic cups). J Appl Polym Sci 96:516–522. https://doi.org/10.1002/app.21474

Fouckhardt H, Steingoetter I, Brinkmann M et al (2007) Nm- and µm-scale surface roughness on glass with specific optical scattering characteristics on demand. Adv Optoelectron. https://doi.org/10.1155/2007/27316

Gonçalves SM, dos Santos DC, Motta JFG et al (2019) Structure and functional properties of cellulose acetate films incorporated with glycerol. Carbohydr Polym 209:190–197. https://doi.org/10.1016/j.carbpol.2019.01.031

Gopi S, Pius A, Kargl R et al (2019) Fabrication of cellulose acetate/chitosan blend films as efficient adsorbent for anionic water pollutants. Polym Bull 76:1557–1571. https://doi.org/10.1007/s00289-018-2467-y

Hansson PM, Skedung L, Claesson PM et al (2011) Robust hydrophobic surfaces displaying different surface roughness scales while maintaining the same wettability. Langmuir 27:8153–8159. https://doi.org/10.1021/la201121p

Harini K, Sukumar M (2019) Development of cellulose-based migratory and nonmigratory active packaging films. Carbohydr Polym 204:202–213. https://doi.org/10.1016/j.carbpol.2018.10.018

Ivanovska A, Cerovic D, Tadic N et al (2019) Sorption and dielectric properties of jute woven fabrics: effect of chemical composition. Ind Crop Prod 140:111632. https://doi.org/10.1016/j.indcrop.2019.111632

Kamide K (ed) (2005) Cellulose and cellulose derivatives. Molecular characterization and its applications. Elsevier, New York

Kamide K, Saito M (1985) Thermal analysis of cellulose acetate solids with total degrees of substitution of 0.49, 1.75, 2.46, and 2.92. Polym J 17:919–928

Karimi K, Taherzadeh MJ (2016) A critical review of analytical methods in pretreatment of lignocelluloses: composition, imaging, and crystallinity. Bioresour Technol 200:1008–1018. https://doi.org/10.1016/j.biortech.2015.11.022

Kennedy JF, Phillips GO, Williams PA, Piculell L (eds) (1995) Cellucon '93 proceedings cellulose and cellulose derivatives: physico-chemical aspects and industrial applications. Woodhead Publishing Limited, Cambridge

Liu H, Lo HY (2002) Ultrafine fibrous cellulose membranes from electrospinning of cellulose acetate. J Polym Sci Part B Polym Phys 40:2119–2129. https://doi.org/10.1002/polb.10261

Liu P, Bai X, Xing W et al (2021) Translucent and superhydrophobic glass for self-cleaning and acid rain-restraining. Mater Chem Phys 259:124049. https://doi.org/10.1016/j.matchemphys.2020.124049

Lyytikäinen J, Morits M, Österberg M et al (2021) Skin and bubble formation in films made of methyl nanocellulose, hydrophobically modified ethyl(hydroxyethyl)cellulose and microfibrillated cellulose. Cellulose 28:787–797. https://doi.org/10.1007/s10570-020-03557-0

Menachem L (ed) (2007) Handbook of fiber chemistry. CRC Press Taylor & Francis Group, Boca Raton

Mikaeili F, Gouma PI (2018) Super water-repellent cellulose acetate mats. Sci Rep 8:1–8. https://doi.org/10.1038/s41598-018-30693-2

Mirvakili MN, Hatzikiriakos SG, Englezos P (2021) Opaque and translucent films from aqueous microfiber suspensions by evaporative self-assembly. Phys Fluids. https://doi.org/10.1063/5.0043881

Mustafa F, Andreescu S (2018) Chemical and biological sensors for food-quality monitoring and smart packaging. Foods 7:168. https://doi.org/10.3390/foods7100168

Park S, Baker JO, Himmel ME et al (2010) Cellulose crystallinity index: measurement techniques and their impact on interpreting cellulose performance. Biotechnol Biofuels 3:1–10. https://doi.org/10.1186/1754-6834-3-10

Paunonen S (2013) Strength and barrier enhancements of cellophane and cellulose derivative films: a review. BioResources 8:3098–3121. https://doi.org/10.15376/biores.8.2.3098-3121

Rodríguez FJ, Abarca RL, Bruna JE et al (2019) Effect of organoclay and preparation method on properties of antimicrobial cellulose acetate films. Polym Compos 40:2311–2319. https://doi.org/10.1002/pc.25041

Shivamurthy B, Thimmappa BHS, Purushothama R, Datta Sai GKVD (2019) Electrical conductivity and mechanical properties of dendritic copper particulate polymer films.

Trans Electr Electron Mater 20:99–106. https://doi.org/10.1007/s42341-018-00085-4

Sukhija S, Singh S, Riar CS (2018) Physical, mechanical, morphological, and barrier properties of elephant foot yam starch, whey protein concentrate and psyllium husk based composite biodegradable films. Polym Compos 39:E407–E415. https://doi.org/10.1002/pc.24488

Tee YB, Wong J, Tan MC, Talib RA (2016) Development of edible film from flaxseed mucilage. BioResources 11:10286–10295. https://doi.org/10.15376/biores.11.4.10286-10295

Vartiainen J, Vähä-Nissi M, Harlin A (2014) Biopolymer films and coatings in packaging applications—a review of recent developments. Mater Sci Appl 05:708–718. https://doi.org/10.4236/msa.2014.510072

Vinodhini PA, Sangeetha K, Thandapani G et al (2017) FTIR, XRD and DSC studies of nanochitosan, cellulose acetate and polyethylene glycol blend ultrafiltration membranes. Int J Biol Macromol 104:1721–1729. https://doi.org/10.1016/j.ijbiomac.2017.03.122

Wan Daud WR, Djuned FM (2015) Cellulose acetate from oil palm empty fruit bunch via a one step heterogeneous acetylation. Carbohydr Polym 132:252–260. https://doi.org/10.1016/j.carbpol.2015.06.011

Wu S, Qin X, Li M (2014) The structure and properties of cellulose acetate materials: a comparative study on electrospun membranes and casted films. J Ind Text 44:85–98. https://doi.org/10.1177/1528083713477443

Xie J, Hung YC (2019) Methodology to evaluate the antimicrobial effectiveness of UV-activated TiO_2 nanoparticle-embedded cellulose acetate film. Food Control. https://doi.org/10.1016/j.foodcont.2019.06.016

Yadav N, Hakkarainen M (2021) Degradable or not? Cellulose acetate as a model for complicated interplay between structure, environment and degradation. Chemosphere 265:128731. https://doi.org/10.1016/j.chemosphere.2020.128731

Yadollahi R, Dehghani Firouzabadi M, Mahdavi H et al (2019) How properties of cellulose acetate films are affected by conditions of iodine-catalyzed acetylation and type of pulp. Cellulose 26:6119–6132. https://doi.org/10.1007/s10570-019-02510-0

Yang ZY, Wang WJ, Shao ZQ et al (2013) The transparency and mechanical properties of cellulose acetate nanocomposites using cellulose nanowhiskers as fillers. Cellulose 20:159–168. https://doi.org/10.1007/s10570-012-9796-z

Zugenmaier P (1997) Surface texture: profile method-rules and procedures for the assessment of surface texture (ISO 4288: 1997)

Zugenmaier P (2004) Characteristics of cellulose acetate. Macromol Symp 208:81–166. https://doi.org/10.1002/masy.200450407